JOURNAL OF MATERIALS SCIENCE 30 (1995) 2610–2615

Preparation and characterization of NTC thermistors based on $Fe_{2+\delta}Mn_{1-x-\delta}Ni_xO_4$

M. L. MARTÍNEZ SARRIÓN, M. MORALES
Departament de Química Inorgànica, Universitat de Barcelona, Diagonal 647, 08028 Barcelona, Spain

Single-phase nickel manganese ferrites, $Ni_xMn_{1-x-\delta}Fe_{2+\delta}O_4$, have been prepared by mild heating of solid solutions of nickel–manganese–iron formates obtained by coprecipitation. Dilatometric and X-ray diffraction studies were conducted at different temperatures, showing the different stages of the sintering process of highly densified nickel manganese ferrite ceramics (density, 94%–96%). Granulometric and SEM studies showed that the oxide particles formed agglomerates of 4 μm, with a narrow size distribution. XPS studies showed that Fe^{2+} was oxidized to Fe^{3+} on the ceramic surface. Finally, electrical measurements showed that $Fe_{2.16}Mn_{0.74}Ni_{0.10}O_4$ presented the minimum resistivity (1340 Ωcm). The sensitivity indices were around 4000 K.

1. Introduction

Negative temperature coefficient (NTC) thermistors are semiconducting ceramics that often consist of transition metal ferrites [1] with the general formula $M_{1-\delta}Fe_{2+\delta}O_4$ (M = Ni, Mn, Co, Cu,. . .). The resistivity and electrical stability ($\Delta R/R$) depend on a number of factors, such as composition, divalent iron content, homogeneity, and microstructure of the ceramics.

Among the characteristics of technical interest for thermistors are room temperature resistivity, and resistance–temperature behaviour, which is reflected by the sensitivity index, β

$$\beta = \frac{\ln R_1 - \ln R_2}{(1/T_1) - (1/T_2)} \quad (1)$$

in our case $T_1 = 298$ K and $T_2 = 358$ K. The ferrites have been investigated previously for use in NTC thermistors, particularly MFe_2O_4 (M = Mn, Mg, Zn) [2, 3] but these materials tend to have lower β values than nickel manganites [4–6].

This paper describes the synthesis of $Ni_xMn_{1-x-\delta}Fe_{2+\delta}O_4$ spinels and their characteristics as revealed by X-ray powder diffraction at different temperatures, granulometry, SEM, X-ray photoelectron spectroscopy (XPS), dilatometry, and electrical measurements. The aim of this study was to improve the methods of synthesis and thermistors characteristics such as microstructure, density and resistivity.

2. Experimental procedure

2.1. Preparation of nickel manganese ferrite powders

Pure solid solutions of formate precursor $Ni_yMn_{1-z-y}Fe_z(O_2CH)_2 \cdot 2H_2O$ were prepared by coprecipitation in water–ethanol (70:30) solution from $NiCl_2 \cdot 6H_2O$, $MnCl_2 \cdot 4H_2O$, and $FeCl_2 \cdot 4H_2O$ with ammonium formate (analytical reagent). After 30 min, the precipitate was filtered and washed in water–ethanol (70:30). The crystals were rhombohedral plates with an average size of 10 μm. Different compositions of formate solid solutions were studied (Table I).

The decomposition of the mixed formate was carried out in N_2–O_2 (between 3% and 7% oxygen) mixture between 310 and 370 °C (soaking time 30 min) depending on the manganese and iron content, and followed by treatment at 700 °C and cooling in a neutral atmosphere.

2.2. Preparation of ceramics

The powders were mixed with an organic binder (PVA) and pressed into pellets [6, 7]. The discs were fired at 60 °C h^{-1} up to 500 °C in air and 1300 or 1200 °C in a controlled atmosphere (0%, 5%, 10%, and 22% O_2) at 200 °C h^{-1} and cooled at 50 °C h^{-1}.

X-ray diffraction (XRD) patterns were obtained on a Siemens D500 powder diffractometer using CuK_α radiation, a scan speed of 0.33° min^{-1}, and a range of 5°–60°. XRD at different temperatures was carried out in an Anton Park Camera. The granulometric measurements were carried out with a Horiba Capa-700 particle analyser. XPS spectra were obtained on a Perkin–Elmer PHI 5500-ESCA System using MgK_α radiation with a pressure around 10^{-9} Pa. The analyses of the microstructure (SEM) were carried out with a Hitachi 800-MT and the dilatometrical measurements with a Netzsch 402E dilatometer. NaCl was used as a standard to fit the X-ray pattern, and the lattice parameters of the oxides were calculated with the computer program AFFMAIL [8].

0022–2461

3. Results and discussion

The composition of the solid solutions which were prepared of general formula $Ni_yMn_{1-z-y}Fe_z(O_2CH)_2 \cdot 2H_2O$ ($y = 0.03$–0.26, $z = 0.73$–0.67) are given in Table I. the isostructural nature of nickel, manganese and iron formates was confirmed by the formation of solid solution throughout the composition range. The compositions were established by chemical analysis. Mixed oxides of general formula $Ni_xMn_{1-x-\delta}Fe_{2+\delta}O_4$ were obtained for $0.1 < x < 0.78$ and $0.07 < \delta < 0.18$.

TABLE I Composition of the formate precursors $Fe_zMn_{1-y-z}Ni_y(O_2CH)_2 \cdot 2H_2O$ and the corresponding nickel manganese ferrites $Fe_{2+\delta}Mn_{1-x-\delta}Ni_xO_4$

Formate precursors			Oxides		
Fe	Mn	Ni	Fe	Mn	Ni
0.713	0.221	0.066	2.14	0.66	0.20
0.701	0.162	0.137	2.10	0.49	0.41
0.692	0.102	0.206	2.07	0.31	0.62
0.707	0.035	0.258	2.12	0.10	0.78
0.719	0.247	0.033	2.16	0.74	0.10
0.718	0.183	0.099	2.15	0.55	0.30
0.711	0.123	0.166	2.13	0.37	0.50
0.727	0.071	0.201	2.18	0.21	0.61

3.1. Granulometry and SEM

Cumulative particle-size distribution histograms and scanning electron micrographs of oxides are shown in Figs 1 and 2, respectively. The mixed oxide crystals did not retain the shape of the formate precursor. They occurred as small particles (ca. 1 μm), which were agglomerated to give a narrow size distribution 1–8 μm) centred around 4 μm. In these oxides, agglomeration was augmented with manganese amount and no significant variations took place with iron content. These oxides presented low surface areas (2.99–2.01 $m^2 g^{-1}$).

The density of the ceramics obtained at 1300 °C was between 94% and 96% (porosity 4%–6%) of theoretical density while the oxides sintered at 1200 °C were less densified (89%–93%) (Fig. 3). Density increased with nickel content and no significant variation was observed with iron amount. The calculated density,

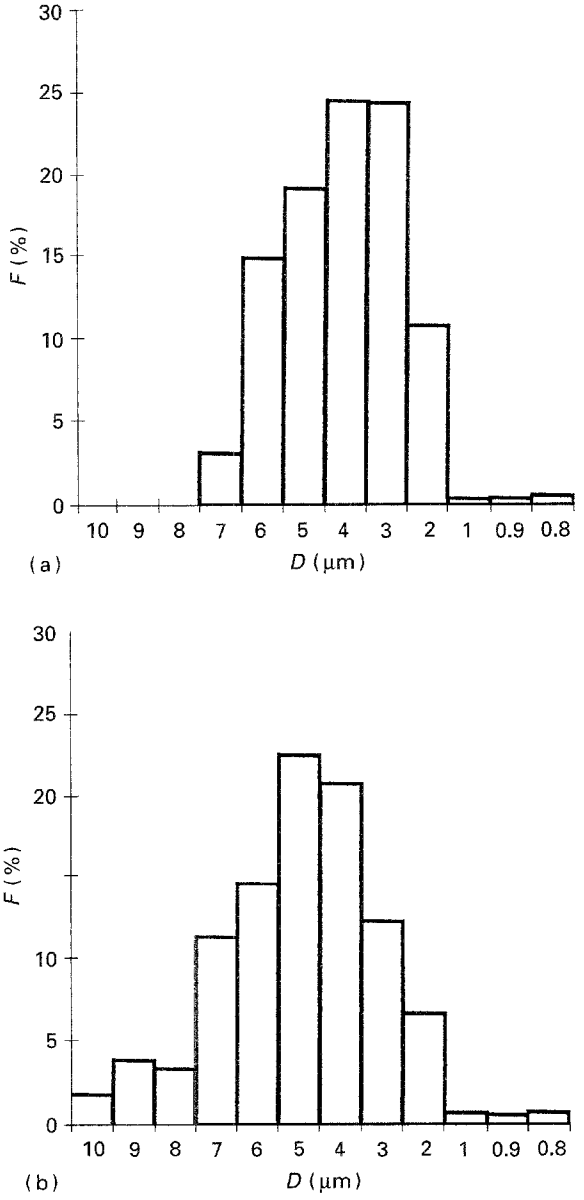

Figure 1 Size distribution histograms of (a) $Fe_{2.18}Mn_{0.21}Ni_{0.61}O_4$, and (b) $Fe_{2.16}Mn_{0.74}Ni_{0.10}O_4$.

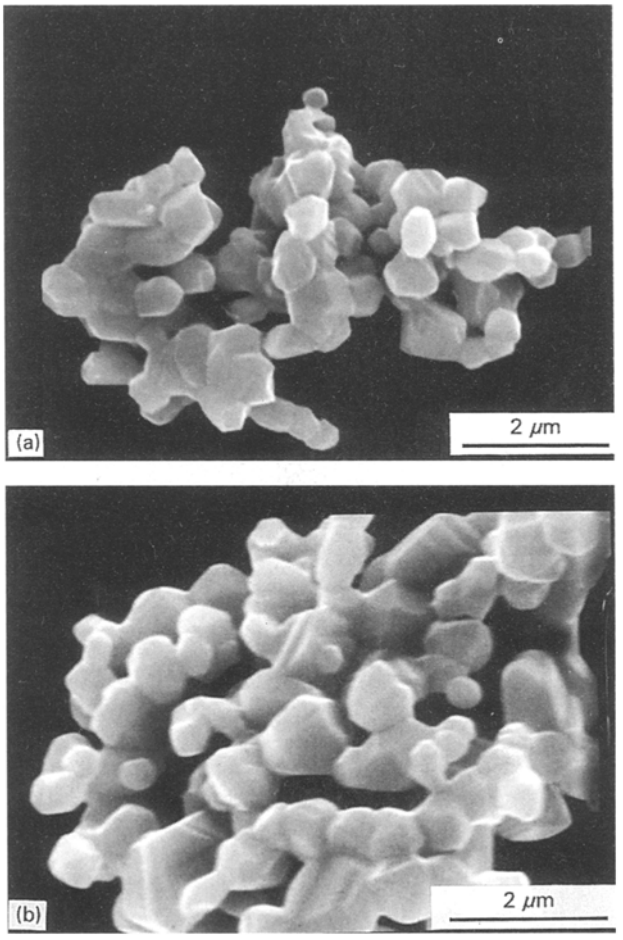

Figure 2 Scanning electron micrographs of (a) $Fe_{2.18}Mn_{0.21}Ni_{0.61}O_4$, and (b) $Fe_{2.16}Mn_{0.74}Ni_{0.10}O_4$.

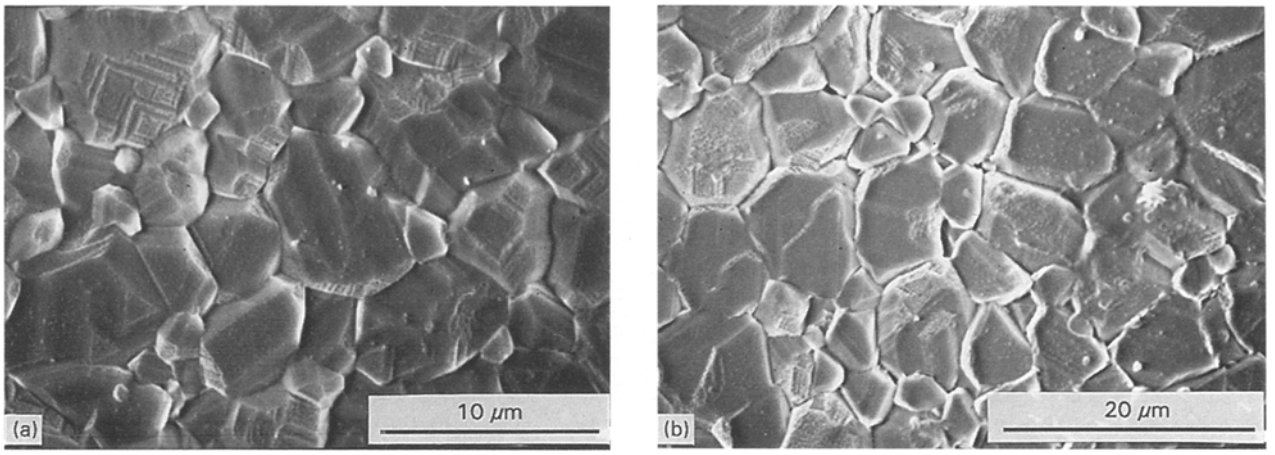

Figure 3 Scanning electron micrographs of ceramics sintered at 1300 °C: (a) $Fe_{2.18}Mn_{0.21}Ni_{0.61}O_4$, and (b) $Fe_{2.16}Mn_{0.74}Ni_{0.10}O_4$. Cooling rate 50 °C h^{-1}.

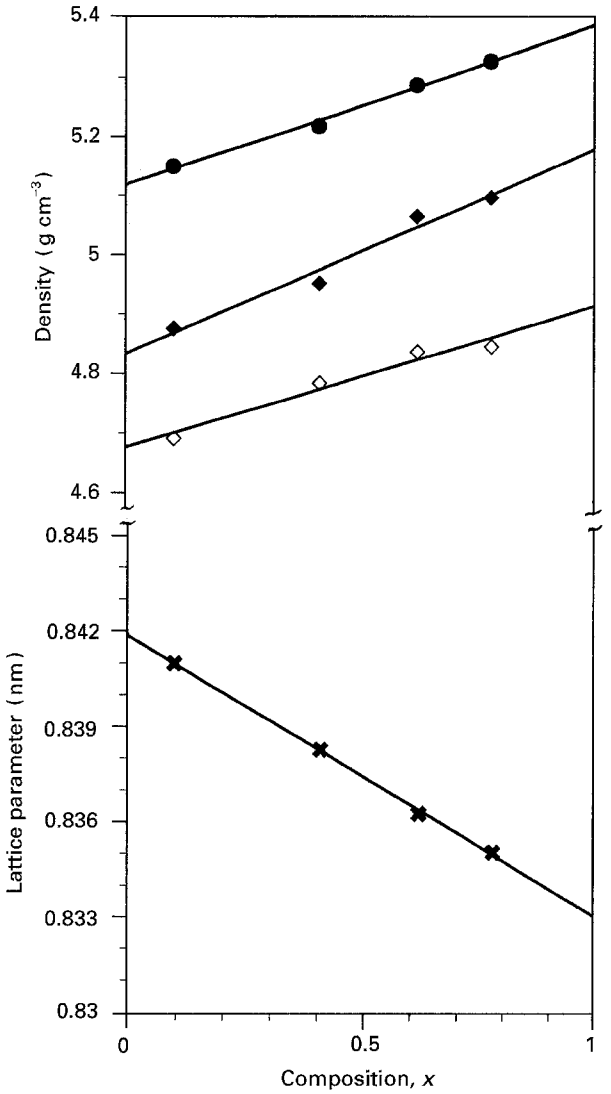

Figure 4 Lattice parameter and densities plotted against oxide composition $[Fe_{2.0+\delta}Mn_{1-x-\delta}Ni_xO_4$ ($\delta \ll 1$)]: (●) d_x = theoretical density determined from XRD, (◇) observed density for ceramics sintered at 1200 °C, (◆) observed density for ceramics sintered at 1300 °C.

d_{XRD}, was obtained from the lattice parameters, a_0, and the apparent density, d_{obs}, was measured (Fig. 4).

$$d_{XRD} = \frac{MZ}{N_A V}$$

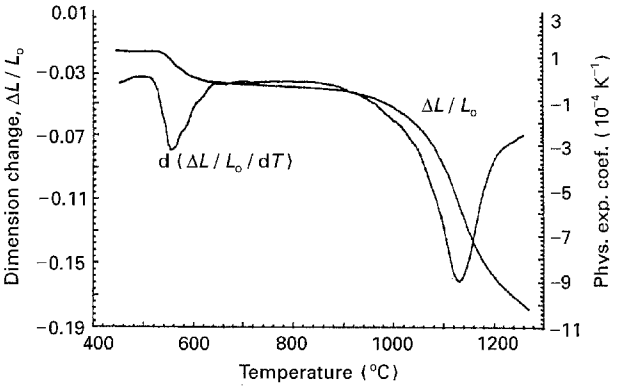

Figure 5 Dilatometric study of $Fe_{2.16}Mn_{0.74}Ni_{0.10}O_4$.

where M is the molecular weight, Z the number of units ($Z = 8$), N_A Avogadro's number and V the unit cell volume ($V = a^3$).

The density of these ceramics was slightly lower than those of nickel manganites sintered under similar conditions [6].

3.2. Dilatometry and XRD at different temperatures

The aim of the dilatometrical measurements was to study the sintering process. The study showed a reaction only during sintering at 560 °C (Fig. 5) which corresponded to a shrinkage ($\Delta L/L_0 = 2.4\%$). Parallel study by XRD at different temperatures showed that this step was related to a partial spinel decomposition to give $(Fe,Mn)_2O_3$ or Fe_2O_3 (Fig. 6b). The percentage of shrinkage corresponded to a 4% reaction. Although, no further steps were observed, XRD on ceramics at 1300 °C only showed spinel phase (Fig. 6c), therefore Fe_2O_3 reduction took place at the end of sintering and was masked by crystal growth which led to fast ceramic shrinkage.

3.3. XPS and resistivity measurements

The literature on XPS characterization of iron oxides includes studies of commercially obtained powders and oxides formed by thermal decomposition of iron and manganese oxalates [9]. There is good agreement

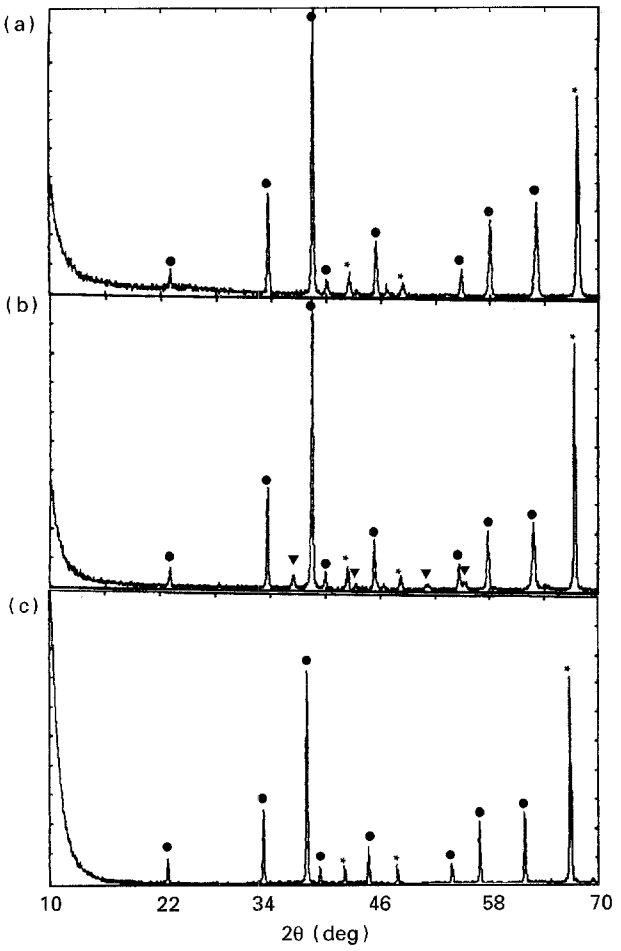

Figure 6 XRD study at different temperatures of $Fe_{2.16}Mn_{0.74}Ni_{0.10}O_4$: (a) room temperature, (b) 700 °C, and (c) 1200 °C. (*) platinum, (●) spinel phase, (▼) Fe_2O_3 or $(Mn, Fe)_2O_3$.

TABLE II Binding energy data for iron and manganese oxides

Compound	$2p_{1/2}$	$2p_{3/2}$	3p	Reference
Fe^{II}_xO	723.8	710.3	–	[11]
Fe^{II}_xO	723.0	709.4	–	[12]
Fe^{II}_xO	722.8	709.5	53.7	[13]
$Fe^{III}_2O_3$	724.6	711.4	–	[11]
$Fe^{III}_2O_3$	724.1	710.5	–	[12]
$Fe^{III}_2O_3$	723.8	710.3	55.3	[13]
$Mn^{II}_2TiO_4$	653.3	641.0	47.4	[14]
$Mn^{II}_2TiO_4$	652.6	640.6	48.0	[15]
$Mn^{II}O$	653.8	642.1	48.2	[16]
$ZnMn^{III}_2O_4$	653.4	641.8	48.3	[14]
$Mn^{III}_2O_3$	653.8	642.1	49.5	[16]

on iron and manganese oxides. A summary of binding energy data is presented in Table II. A number of useful conclusions can be drawn from the table.

(i) Octahedrally and tetrahedrally coordinated Fe(III) species cannot be distinguished by their core-level XPS spectra.

(ii) Fe(III) has a $2p_{3/2}$ binding energy around 711.5 eV in iron oxides, and Fe(II) has a binding energy around 709.7 eV.

(iii) Fe(III) presents a broad shake-up satellite at ~ 719 eV and Fe(II) at ~ 715 eV [10].

(iv) 3p components in iron and manganese oxides have close binding energies, therefore the main peak is a result of $3p_{3/2}$ and $3p_{1/2}$ components.

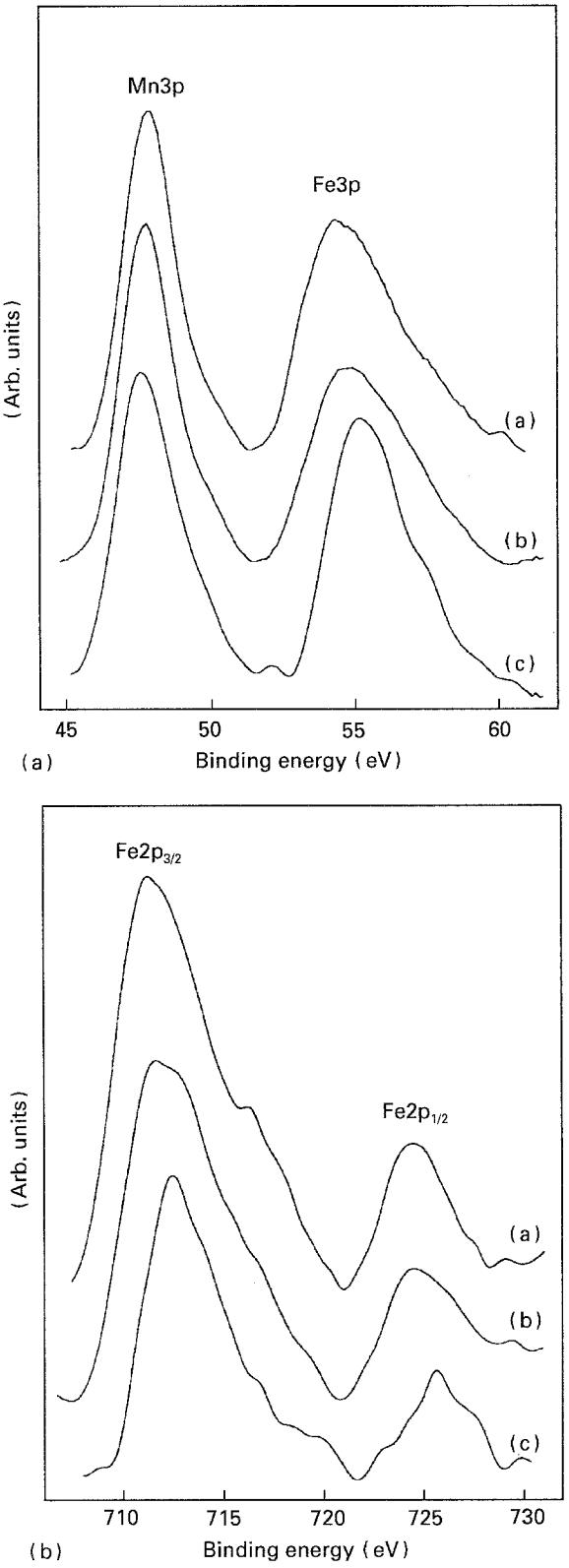

Figure 7 XPS depth profile of Fe 2p, Fe 3p and Mn 3p signals on ceramic $Fe_{2.14}Mn_{0.66}Ni_{0.20}O_4$: after (a) 3 min sputtering, (b) 0.5 min sputtering, and (c) without sputtering.

It is known that surface ferrite powders are oxidized to Fe_2O_3 due to contact with the atmosphere. This has enormous importance in the electrical properties of their NTC thermistors. A depth profile was performed to study this process of $Fe_{2.16}Ni_{0.10}Mn_{0.74}O_4$ ceramic sintered under nitrogen at 1300 °C and cooled at 50 °C h^{-1}. The ceramic surface was sputtered with argon ions, and measurements were taken every

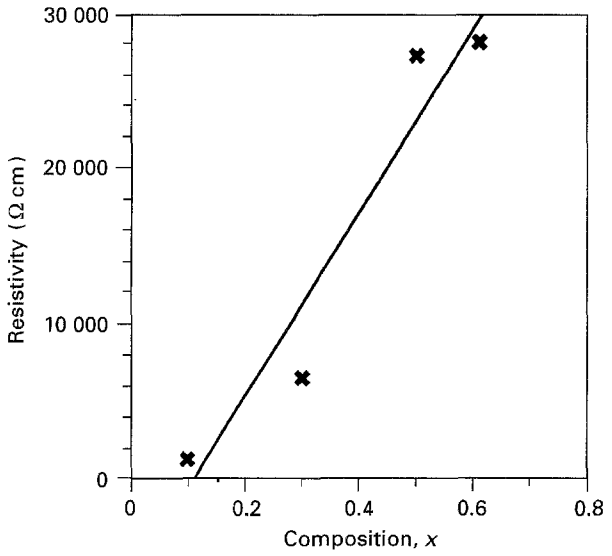

Figure 8 Resistivity versus composition of $Fe_{2.15+\delta}Mn_{0.85-x-\delta}Ni_xO_4$ ($\delta \ll 1$).

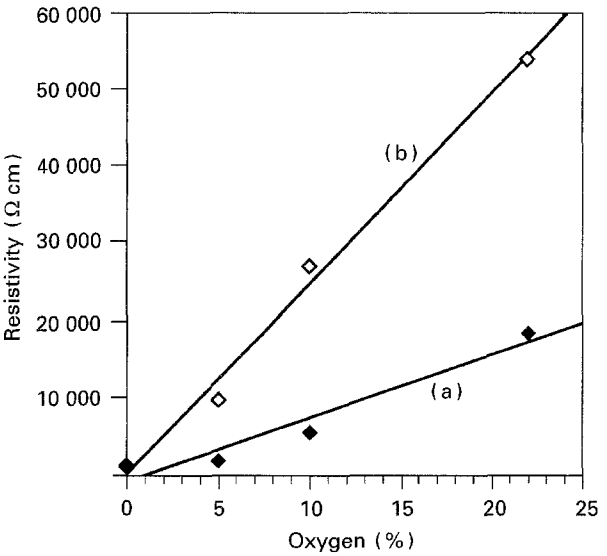

Figure 9 Effect of oxygen content in the sintering atmosphere on samples fired at 1300 °C and cooled to maintain a constant oxygen content. (a) $Fe_{2.14}Mn_{0.66}Ni_{0.20}O_4$, and (b) $Fe_{2.16}Mn_{0.74}Ni_{0.10}O_4$.

0.5 min. The peaks studied were Mn 3p, Mn 2p, Fe 3p and Fe 2p, and Ar $3p_{3/2}$ and C 1s to establish the shifting.

On the ceramic surface (Fig. 7c), iron was present as Fe^{3+}. After 0.5 min sputtering, a partial shift of both 3p and 2p iron peaks to lower energies was observed (Fig. 7b), and after 3 min of sputtering the global shift for iron was around -0.7 eV while manganese peaks were slightly shifted to higher energies (~ 0.2 eV) (Fig. 7a). The fitting of these peaks showed an increase in Fe^{2+}/Fe^{3+} from practically zero to 1/10, which was in agreement with bulk composition, while the Mn^{3+}/Mn^{2+} ratio was almost constant, showing a value of 1/4.

Fe^{2+} and Fe^{3+} in octahedral sites are responsible for conductivity in ferrites [17]. Manganese ferrites present low resistivities and sensitivity indices [3, 17], which cut down their use as NTC thermistors at room temperature. To improve their properties, we introduced Ni^{2+} and sintered at different O_2–N_2 mixtures to modify the Fe^{2+}/Fe^{3+} ratio in the octahedral sites, and the grain-boundary resistivity. The results are shown in Figs 8 and 9. The minimum resistivity corresponded to $Fe_{2.16}Mn_{0.74}Ni_{0.10}O_4$ (1340 Ωcm) and $Fe_{2.14}Mn_{0.66}Ni_{0.2}O_4$ (1633 Ωcm). Both ferrites were sintered under nitrogen. Resistivity increased with the amount of nickel (Fig. 8), because nickel was placed in octahedral sites [17], therefore a decrease in iron content in the octahedral sites took place. Resistivity also increased with oxygen percentage in the sintering atmosphere. This is in agreement with XPS measurements where oxidation of Fe^{2+} to Fe^{3+} on the surface was observed. Surface oxidations lead to an increase in device resistivity [18]. This oxidation process was diminished increasing nickel content in the ferrites (Fig. 9). The sensitivity index, β, for these oxides was between 3800 and 4100 K, which is similar to nickel manganites [6].

Electrical stability studies, $\Delta R/R$, on $Fe_{2.16}Mn_{0.74}Ni_{0.10}O_4$ and $Fe_{2.14}Mn_{0.66}Ni_{0.20}O_4$ (Fig. 10) showed that ferrites with higher nickel contents were the most

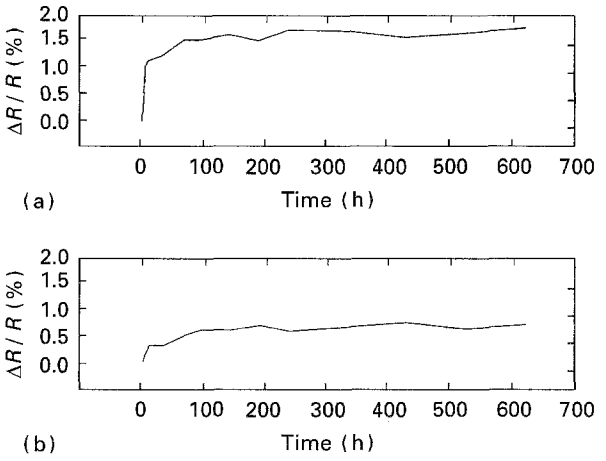

Figure 10 Resistance variation, $\Delta R/R$, against time at 25 °C: (a) $Fe_{2.16}Mn_{0.74}Ni_{0.10}O_4$, and (b) $Fe_{2.14}Mn_{0.66}Ni_{0.20}O_4$. Ageing temperature 105 °C.

stable. These oxides presented an electrical stability similar to nickel manganites and nickel manganites doped with lithium [6, 7].

4. Conclusions

1. Solid solutions of $Ni_yMn_{1-z-y}Fe_z(O_2CH)_2 \cdot 2H_2O$ were precipitated from their chloride solutions with ammonium formate.

2. The thermal decomposition of these solid solutions led to nickel manganese ferrites in mild conditions.

3. The oxide particles had a size around 1 μm, but were slightly agglomerated.

4. Ceramics sintered at 1300 °C presented higher densities. The density of these ceramics diminished with manganese content.

5. A partial decomposition of ferrite during the sintering process to give Fe_2O_3 was observed by dilatometry and XRD at 560 °C, although at the end

of the sintering process, spinel phase was the only phase present.

6. XPS studies showed that Fe^{2+} was oxidized to Fe^{3+} on the ceramic surface.

7. Resistivity measurements indicated that ferrites with high manganese content presented low resistivities with high sensitivity indices which made them useful as NTC thermistors.

Acknowledgements

The authors thank Professor A. Rousset (LCMI), University Paul Sabatier (Toulouse, France), for his assistance, and Serveis Científico-tècnics, University of Barcelona. This work was partially sponsored by financial support from DGICYT PB90-0029, and DGU (Generalitat de Catalunya) through a fellowship.

References

1. D. G. HILL and H. L. TULLER, "Ceramic Materials for Electronics. Processing, Properties, and Applications", edited by R. C. Buchanan (Marcel Dekker, New York, 1986) Ch. 5.
2. A. BECKER, C. B. GREEN and G. L. PEARSON, *Elec. Eng. Trans.* **65** (1946) 711.
3. D. W. JOHNSON Jr, M. ROBBINS, E. M. VOGEL and V. G. LAMBRECHT Jr, *Am. Ceram. Soc. Bull.* **62** (1983) 597.
4. E. JABRY, G. BOISSIER, A. ROUSSET, R. CARNET and A. LAGRANGE, *J. Phys. Coll. C1* **69**, (1982) 325.
5. R. LEGROS, R. METZ, J. P. CAFFIN, A. LAGRANGE and A. ROUSSET, *Mater. Res. Soc. Symp. Proc.* **121** (1988) 251.
6. M. L. MARTÍNEZ SARRIÓN and M. MORALES, *J. Mater. Chem.* **3** (1993) 273.
7. *Idem, J. Am. Ceram. Soc.* submitted.
8. J. STEWART, "AFFMAIL, a computer program for cell-parameters refinement", University of Bordeaux (1970); modified by J. Rodriguez Carvajal (1985).
9. U. LINDER, and H. PAPP, *Appl. Surf. Sci.* **32** (1988) 75.
10. C. S. KUIVILA, J. B. BUTT and P. C. STAIR, *ibid.* **32** (1988) 99.
11. G. C. ALLEN, M. T. CURTIS, A. J. HOOPER and P. M. TUCKER, *J. Chem. Soc. Dalton Trans.* (1974) 1525.
12. K. HIROKAWA and M. OKU, *Tantala* **26** (1979) 855.
13. S. VASUDEVAN, M. S. HEDGE and C. N. R. RAO, *J. Solid State Chem.* **29** (1979) 253.
14. J. TÖPFER, A. FELTZ, D. GRÄF, B. HACKL, L. RAUPACH and P. WEISSBRODT, *Phys. Status Solidi (a)* **134** (1992) 405.
15. V. A. M. BRABERS, F. M. VAN SETTEN and P. S. A. KNAPEN, *J. Solid State Chem.* **49** (1983) 93.
16. M. JORGES-SOARES, F. MEMMES, R. FONTAINE and R. CAILLAT, *C. R. Acad. Sci. (Fr)* **294** (1987) 549.
17. HAN ILL YOO, and H. L. TULLER, *J. Am. Ceram. Soc.* **70** (1987) 388.

Received 3 March
and accepted 14 November 1994